

Bistatic OFDM-based Joint Radar-Communication: Synchronization, Data Communication and Sensing

Lucas Giroto de Oliveira^{†*}, David Brunner[†], Axel Diewald[†],

Charlotte Muth[‡], Laurent Schmalen[‡], Thomas Zwick[†], and Benjamin Nuss[†]

[†]Institute of Radio Frequency Engineering and Electronics (IHE), [‡]Communications Engineering Lab (CEL)

Karlsruhe Institute of Technology (KIT), Germany

E-mail: *lucas.oliveira@kit.edu

Abstract—This article introduces a bistatic joint radar-communication (RadCom) system based on orthogonal frequency-division multiplexing (OFDM). In this context, the adopted OFDM frame structure is described and system model encompassing time, frequency, and sampling synchronization mismatches between the transmitter and receiver of the bistatic system is outlined. Next, the signal processing approaches for synchronization and communication are discussed, and radar sensing processing approaches using either only pilots or a reconstructed OFDM frame based on the estimated receive communication data are presented. Finally, proof-of-concept measurement results are presented to validate the investigated system and a trade-off between frame size and the performance of the aforementioned processing steps is observed.

Index Terms—Bistatic radar, orthogonal frequency-division multiplexing (OFDM), joint radar-communication (RadCom).

I. INTRODUCTION

In addition to progressively scarce spectral resources and convergent hardware development, the increasing demand for higher data rates in communication systems and the need for coordinating non-collocated users in modern radar systems have driven efforts towards the development of joint radar-communication (RadCom) systems. In this context, the simultaneous use of waveforms such as orthogonal frequency-division multiplexing (OFDM) for radar sensing and communication has been widely investigated [1].

To increase the diversity of radar measurements in OFDM-based RadCom systems, bistatic measurements can be performed additionally to monostatic sensing. If hardware-level synchronization is not possible, preamble symbols and pilot subcarriers can be used to perform over-the-air synchronization of a non-collocated transmitter-receiver pair. In this article, the latter approach is mathematically formulated and a complete system model for a bistatic OFDM-based RadCom system is outlined. Finally, proof-of-concept measurement results are presented and discussed to illustrate the carried-out discussion and validate the investigated system.

II. SYSTEM MODEL

In the considered bistatic single-input single-output (SISO) OFDM-based RadCom system, a frame $\mathbf{X} \in \mathbb{C}^{N \times M}$ with $M \in \mathbb{N}_{>0}$ OFDM symbols, each with $N \in \mathbb{N}_{>0}$ subcarriers, is designed at the transmitter side in discrete-frequency domain. Out of the total of M OFDM symbols, $M_{\text{pb}} \in \mathbb{N}_{>0}$ are preamble and $M_{\text{pl}} \in \mathbb{N}_{>0}$ payload (PL) symbols. Within the PL

symbols, pilot subcarriers are reserved for channel estimation at the receiver side in a hybrid comb-block arrangement [2], where the spacing in number of subcarriers within pilots in an OFDM symbol is $\Delta N_{\text{pil}} \in \mathbb{N}_{>0}$ and the spacing between OFDM symbols containing pilots is of $\Delta M_{\text{pil}} \in \mathbb{N}_{>0}$ OFDM symbols. As discussed in [2], ΔN_{pil} and ΔM_{pil} will limit the maximum propagation delay and Doppler shift that can be estimated with the pilot OFDM subcarriers, respectively. The adopted OFDM frame structure is depicted in Fig. 1.

Once the discrete-frequency domain OFDM frame is designed, each of its OFDM symbols undergoes a inverse discrete Fourier transform (IDFT) and has a cyclic prefix (CP) of length $N_{\text{CP}} \in \mathbb{N}_{>0}$ prepended to it. This results in a discrete-time domain OFDM frame that is ultimately transformed into the transmit sequence $x[n] \in \mathbb{C}$, $n \in \mathbb{Z}$, via paralell-to-serial (P/S) conversion. This sequence contains all $(N + N_{\text{CP}})(M_{\text{pb}} + M_{\text{pl}})$ samples, which include preamble, pilots for channel estimation and PL. Before transmission, the real and imaginary parts of $x[n]$ undergo digital-to-analog (D/A) conversion with sampling rate F_s , generating the continuous-time domain baseband transmit signal $x(t) \in \mathbb{C}$ that occupies a bandwidth $B \leq F_s$.

The signal $x(t)$ then undergoes analog conditioning and

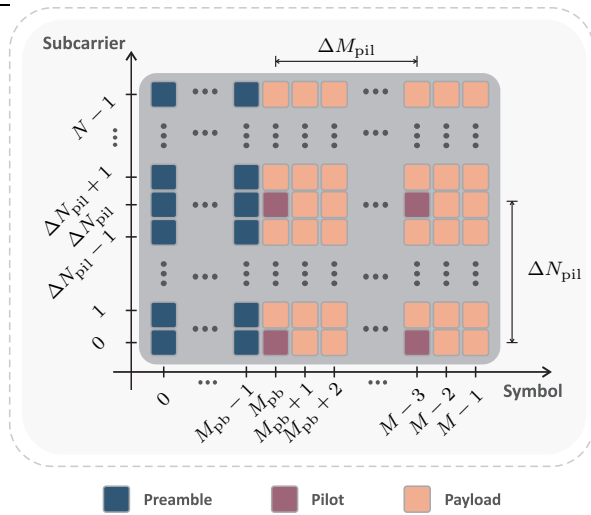


Fig. 1. Structure of the OFDM frame \mathbf{X} in the discrete-frequency domain.

upconversion to a carrier frequency $f_c \gg B$ in an I/Q analog front-end (AFE), being finally radiated by the transmit antenna. After propagation, the OFDM signal is received at the receive antenna, undergoing conditioning and downconversion to the baseband in the receive AFE. The resulting continuous-time domain baseband receive signal without noise, which is denoted by $\tilde{y}(t) \in \mathbb{C}$, can be expressed as

$$\begin{aligned} \tilde{y}(t) = & \alpha^{\text{main}} x(t - \tau_{\text{main}} - \tau_\Delta) e^{j2\pi f_{D,\text{main}} t} e^{j(2\pi f_\Delta t + \phi_\Delta)} \\ & + \sum_{p=0}^{P_{\text{sec}}-1} \alpha_p^{\text{sec}} x(t - \tau_{\text{sec},p} - \tau_\Delta) e^{j2\pi f_{D,\text{sec},p} t} e^{j(2\pi f_\Delta t + \phi_\Delta)}. \end{aligned} \quad (1)$$

In this equation, it is assumed that the OFDM signal propagates through a main path, which can, e.g., be a line-of-sight (LoS) path, and has attenuation α^{main} , delay τ_{main} , and Doppler shift $f_{D,\text{main}}$. Additionally, the transmit OFDM signal propagates through $P_{\text{sec}} \in \mathbb{N}$ secondary paths labeled as $p \in \{0, 1, \dots, P_{\text{sec}} - 1\}$. Each p th path has more severe attenuation than the main one, i.e., $\alpha_p^{\text{sec}} \ll \alpha^{\text{main}}$, and experiences delay $\tau_{\text{sec},p}$, and Doppler shift $f_{D,\text{sec},p}$. Besides both the contributions of the main and secondary paths, $\tilde{y}(t)$ suffers from synchronization mismatches due to the use of distinct clock sources and local oscillator (LO) signals in the non-collocated transmitter and receiver of the bistatic SISO OFDM-based RadCom system. Among these mismatches are the symbol time offset (STO) τ_Δ caused by the unknown transmitter time reference at the receiver, as well as the carrier frequency offset (CFO) f_Δ and its resulting carrier phase offset (CPO) ϕ_Δ between the transmit and receive oscillators.

After the aforementioned analog conditioning, the continuous-time domain baseband receive signal $\tilde{y}(t)$ is impaired by noise and then sampled at the receiver side with a sampling rate that should ideally be equal to F_s . In practice, however, a sampling frequency offset (SFO) w.r.t. the transmitter is experienced since the sampling clock at the receiver is not synchronous to the one at the transmitter. Consequently, the resulting discrete-time domain sequence $y[n] \in \mathbb{C}$ from the analog-to-digital (A/D) conversion on noise-impaired version of $\tilde{y}(t)$ can be expressed as

$$y[n] = \tilde{y}(nT_s(1 + \delta)) + w[n], \quad (2)$$

where $\delta \in \mathbb{R}$ is the SFO normalized by F_s [3], and $w[n] \in \mathbb{C}$ is the sampled additive white Gaussian noise (AWGN).

III. RADAR AND COMMUNICATION SIGNAL PROCESSING

Before the receiver of the bistatic SISO OFDM-based RadCom system extracts communication data and forms a bistatic radar image from $y[n]$, the aforementioned synchronization mismatches are corrected as follows. First, $M_{\text{S&C}} = 2$ preamble OFDM symbols are used by the Schmidl & Cox (S&C) algorithm [4] to find a coarse start point estimate of the OFDM frame in $y[n]$, as well as a CFO estimate. After correcting the CFO only for the approximate region around the preamble OFDM symbols for reduced complexity, a fine estimation of the OFDM frame start point is performed

via cross-correlation in the discrete-time domain between the aforementioned section of $y[n]$ and a copy of the originally transmitted first preamble OFDM symbol. This is similar to the processing in [2], except for the prior CFO correction that is necessary to avoid degradation of the correlation pattern if high frequency shifts are experienced.

Afterwards, SFO is estimated via the use of multiple pairs of identical OFDM symbols, which constitute a total of $M_{\text{SFO}} \in \mathbb{N}_{>0}$ OFDM symbols such that $\langle M_{\text{SFO}} \rangle_2 = 0$, where $\langle \cdot \rangle_2$ is the modulo 2 operator. Combined with the preamble symbols for the S&C algorithm, these symbols constitute the preamble of the OFDM frame, i.e., $M_{\text{pb}} = M_{\text{S&C}} + M_{\text{SFO}}$. At the receiver side, the OFDM symbols at the corresponding positions to these M_{SFO} preamble symbols are fed to the weighted least-squares algorithm proposed by Tsai et al. in [5] to estimate the normalized SFO δ . To correct the SFO, the obtained estimate is fed to a resampling algorithm, which in this article consists of an interpolator based on a multirate finite impulse response (FIR) filter, a sample rate converter based on a polynomial filter, and a decimator based on another multirate FIR filter. After correcting the SFO, the discrete-time domain samples corresponding to the M_{pb} preamble OFDM symbols are discarded and the CFO estimated with the S&C algorithm is corrected for the M_{pl} PL OFDM symbols.

Once STO, CFO, and SFO have been corrected, serial-to-paralell (S/P) conversion can be performed on the resulting sequence containing the M_{pl} PL OFDM symbols to generate a discrete-time domain OFDM frame with CPs. The CPs are then removed from the symbols at the columns of the aforementioned frame and column-wise discrete Fourier transform (DFT) is performed to generate the discrete-frequency domain frame denoted by $\mathbf{Y} \in \mathbb{C}^{N \times M_{\text{pl}}}$. The subcarriers in \mathbf{Y} at the corresponding positions of the allocated pilots at the transmitter side can then be evaluated to

- 1) Estimate and correct Doppler shifts experienced by the OFDM signal during propagation through the main path.
- 2) Estimate the full channel frequency response (CFR) matrix for the OFDM frame via interpolation of its known elements estimated at pilot subcarriers.
- 3) Compensate the residual SFO after the aforementioned correction. This is done by estimating the linearly progressing change in the delay of the main path along subsequent OFDM symbols via the obtained channel estimates with pilot subcarriers and accordingly aligning the OFDM symbols as described in [6], while also updating the corresponding CFR estimates.

After the aforementioned corrections, channel equalization is carried out and data is finally extracted from the PL OFDM subcarriers, which completes the communication signal processing and enables generating a bistatic radar image.

If one cannot ensure that the modulation symbols are correctly received, only the CFR matrix elements at the positions of pilot subcarriers undergo range-Doppler processing to generate a radar image. This will result reduced performance due to the use of interleaved OFDM subcarriers [1], [2] and to the fact that not all PL OFDM symbols will be used for

TABLE I: Radar performance parameters in the considered bistatic OFDM-based RadCom system

Processing gain	$G_p = (N/\Delta N_{\text{pil}})(M_{\text{pl}}/\Delta M_{\text{pil}})$
Range resolution	$\Delta R = c_0/B$
Max. unamb. range	$R_{\max,\text{ua}} = (N/\Delta N_{\text{pil}}) c_0/B$
Max. ISI-free range	$R_{\max,\text{ISI}} = N_{\text{CP}} c_0/B$
Doppler shift resolution	$\Delta f_D = B/[(N + N_{\text{CP}}) M_{\text{pl}}]$
Max. unamb. Doppler shift	$f_{D,\max,\text{ua}} = B/[2\Delta M_{\text{pil}}(N + N_{\text{CP}})]$
Max. ICI-free Doppler shift	$f_{D,\max,\text{ICI}} = B/(10N)$

radar sensing if $\Delta M_{\text{pil}} > 1$. If, however, approximately error-free data communication can be guaranteed, e.g., with channel coding, then the full CFR matrix can be estimated based on the knowledge of the content of all transmit subcarriers. Unlike the sole use of pilot subcarriers, this results in the full achievable performance in terms of processing gain, maximum unambiguous range, and maximum unambiguous Doppler shift of an OFDM radar, which are achieved adopting $\Delta N_{\text{pil}} = 1$ and $\Delta M_{\text{pil}} = 1$. The bistatic radar performance parameters based on the radio-frequency (RF) and OFDM signal parameters are presented in Table I. These parameters can be derived from similar calculations to those in the monostatic case [1]. As a bistatic Doppler shift results from the sum of the Doppler shifts associated with the projections of the target’s velocity vector onto the transmitter-target and receiver-target directions, Doppler shift is considered instead of velocity.

IV. MEASUREMENT SETUP AND RESULTS

In this section, a performance analysis of the considered bistatic OFDM-based RadCom system is performed. For that purpose, a measurement setup with two Zynq UltraScale+ RFSoC ZCU111 system-on-a-chip (SoC) platforms from Xilinx, Inc, was used. One ZCU111 was used to emulate the transmitter of the bistatic OFDM-based RadCom system, while the other one was used to emulate both the receiver and the radar target simulator (RTS) described in [7]. The boards were connected via coaxial cables and power combiners/splitters so that a main, stronger LoS path between transmitter and receiver and a moving target could be emulated at an intermediate frequency (IF). Although no RF AFEs were used for an actual over-the-air transmission, STO, CFO, and SFO were still experienced due to the distinct time references as well as the use of 1 GHz digital IFs and sampling clocks originated from distinct phase-locked loops (PLLs) at the transmitter and receiver. For both boards, $B = 1 \text{ GHz}$ and a digital IF of 1 GHz were used. Additionally, the variants of OFDM signal parameterization with short and long PLs and their resulting performance parameters listed in Table II were adopted.

Fig. 2(a) shows the estimated channel impulse response (CIR) matrix between the first SFO correction via resampling based on the estimate from the Tsai algorithm and the subsequent residual SFO compensation for the long PL case ($M_{\text{pl}} = 4096$). At the first PL symbol, the LoS path is at a relative delay of 0 ns since it is aligned to the S&C estimated

TABLE II: Adopted OFDM signal parameters and resulting radar performance parameters

	Long PL	Short PL
OFDM signal parameters		
No. of subcarriers (N)	2048	
CP length (N_{CP})	512	
No. of preamble symbols ($M_{\text{S\&C}}, M_{\text{SFO}}$)	2, 10	
No. of PL symbols (M_{pl})	4096	512
Pilot spacing ($\Delta N_{\text{pil}}, \Delta M_{\text{pil}}$)	2, 4	
Communication performance parameters		
Channel coding and code rate	LDPC, 2/3	
Data rate (100% duty cycle, $\mathcal{R}_{\text{comm}}$)	0.93 Gbit/s	0.91 Gbit/s
Radar performance parameters		
Processing gain (G_p)	60.21 dB (pilot only) 69.24 dB (full)	51.18 dB (pilot only) 60.21 dB (full)
Range resolution (ΔR)	0.30 m	
Max. unamb. range ($R_{\max,\text{ua}}$)	307.2 m (pilot) 614.4 m (full)	
Max. ISI-free range ($R_{\max,\text{ISI}}$)	153.6 m	
Doppler shift resolution (Δf_D)	95.37 Hz	762.94 Hz
Max. unamb. Doppler shift ($f_{D,\max,\text{ua}}$)	48.83 kHz (pilot) 195.31 kHz (full)	
Max. ICI-free Doppler shift ($f_{D,\max,\text{ICI}}$)	48.83 kHz	

frame start. In its turn, the emulated target, which is partly shadowed by the sidelobes of the LoS path, is at a relative delay of around 7.25 ns w.r.t. the LoS path in the first PL symbol. As the PL symbol index increases, a linear migration is observed for the relative delays. This effect is due to the fact that a residual SFO still remains after SFO estimation with the algorithm proposed by Tsai et al. in [5] and correction via resampling. For the short PL case ($M_{\text{pl}} = 512$), the delay migration would be significantly reduced due to its shorter frame duration, which does not allow significant accumulation of the imposed delay by the residual SFO. In both cases, the delay migration becomes nearly negligible if compensated following the approach described in [6]. Besides delay migration, frequency shift migration is also experienced along the OFDM subcarriers due to the residual SFO [3]. This is shown in Fig. 2(b) for the long PL case, where the LoS path and the emulated target assume frequency shifts of around -14.04 kHz and -19.35 kHz at the leftmost subcarrier, respectively. Due to the residual SFO, these frequency shifts migrate along the subcarrier axis. The processing from [6], however, cannot correct the experienced frequency shift migration.

Next, the normalized densities of the receive quadrature phase-shift keying (QPSK) constellations are shown in Fig. 3. Despite equivalent synchronization performance, the constellation is more diffuse in the long PL case than for short PL since the residual SFO correction can only compensate the delays to a certain extent, but not the attenuation of subcarriers and the cumulative intercarrier interference (ICI) that causes frequency shift migration [3] that becomes more significant over time.

Finally, the obtained range-Doppler radar images using the full frame after reliably estimating the received PL QPSK symbols via low-density parity-check (LDPC) decoding and

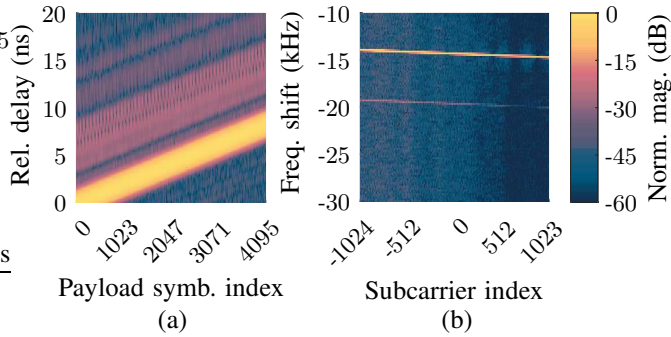


Fig. 2. Migration of (a) delay and (b) frequency shift after time, frequency and sampling frequency synchronization with the S&C and Tsai algorithms and before residual SFO compensation for long PL ($M_{pl} = 4096$).

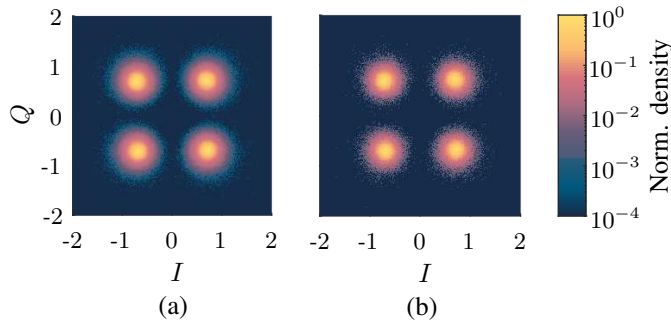


Fig. 3. Receive QPSK constellations: (a) long PL ($M_{pl} = 4096$) and (b) short PL ($M_{pl} = 512$).

Hamming windowing in range and Doppler directions are shown in Fig. 4. During the measurements, the transfer functions of digital-to-analog and analog-to-digital converters, as well as cables have not been calibrated, which led to additional reflections in the range direction. While a negligible residual time offset after synchronization and therefore range offset was experienced, a somewhat inaccurate frequency synchronization with the S&C algorithm resulted in a Doppler shift offset of -0.40 kHz in the obtained radar images. Moreover, comparing the results from Figs. 4(a) and 4(b), one can see that a slightly higher range migration, which results from the previously discussed delay migration, is observed in the long PL case in the form of wider peaks in the range direction. This happens due to the limited accuracy of the delay estimation used for compensation with the approach from [6]. Additionally, it can be seen that the residual SFO prevents windowing in Doppler direction from appropriately suppressing sidelobes. While this results in a blurs around the peaks in Doppler direction for the short PL case in Fig. 4(b), additional sidelobes appear along the Doppler shift axis in Fig. 4(a) due to the accumulated residual SFO effect over time in the long PL case.

V. CONCLUSION

This article has discussed the processing chain of a bistatic SISO OFDM-based RadCom system, including a synchronization procedure and a brief description of both communication and radar signal processing steps. The presented results have demonstrated the effects of residual synchronization mismatches on both the receive constellations and the

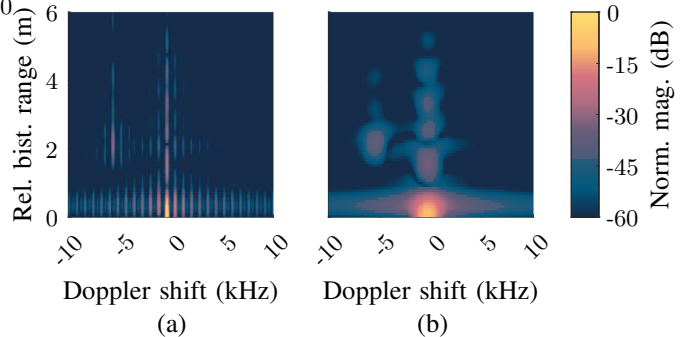


Fig. 4. Range-Doppler radar images: (a) long PL ($M_{pl} = 4096$) and (b) short PL ($M_{pl} = 512$).

obtained range-Doppler radar images. More specifically, it was observed that residual time and frequency offsets yield range and Doppler offsets, respectively, whereas residual sampling frequency offsets result in range and Doppler migration. Focusing on SFO, it was shown that an existing technique in the literature is able to sufficiently compensate for range migration, while the correction of Doppler shift migration remains an open issue. Finally, since only relative bistatic ranges to a stronger path can be estimated, the length of the main path must be known. This is, e.g., possible via an LoS link between two fixed base stations or by estimating the distance between the bistatic pair via monostatic radar measurements in an automotive radar.

ACKNOWLEDGMENT

The authors acknowledge the financial support by the Federal Ministry of Education and Research of Germany in the projects “KOMSENS-6G” (grant number: 16KISK123) and “Open6GHub” (grant number: 16KISK010). The work of Lucas Giroto de Oliveira was also financed by the German Academic Exchange Service (DAAD) - Funding program 57440921/Pers. Ref. No. 91555731.

REFERENCES

- [1] L. Giroto de Oliveira, B. Nuss, M. B. Alabd, A. Diewald, M. Pauli, and T. Zwick, “Joint radar-communication systems: Modulation schemes and system design,” *IEEE Trans. Microw. Theory Tech.*, vol. 70, no. 3, pp. 1521–1551, Mar. 2022.
- [2] Y. L. Sit, B. Nuss, and T. Zwick, “On mutual interference cancellation in a MIMO OFDM multiuser radar-communication network,” *IEEE Trans. Veh. Technol.*, vol. 67, no. 4, pp. 3339–3348, Dec. 2018.
- [3] L. Smaini, “RF analog impairments description and modeling,” in *RF Analog Impairments Modeling for Communication Systems Simulation: Application to OFDM-based Transceivers*. John Wiley & Sons, Ltd, 2012, ch. 2, pp. 37–105.
- [4] T. M. Schmidl and D. C. Cox, “Robust frequency and timing synchronization for OFDM,” *IEEE Trans. Commun.*, vol. 45, no. 12, pp. 1613–1621, Dec. 1997.
- [5] P.-Y. Tsai, H.-Y. Kang, and T.-D. Chiueh, “Joint weighted least-squares estimation of carrier-frequency offset and timing offset for OFDM systems over multipath fading channels,” *IEEE Trans. Veh. Technol.*, vol. 54, no. 1, pp. 211–223, 2005.
- [6] F. Burmeister, R. Jacob, A. Traßl, N. Schwarzenberg, and G. Fettweis, “Dealing with fractional sampling time offsets for unsynchronized mobile channel measurements,” *IEEE Wireless Commun. Lett.*, vol. 10, no. 12, pp. 2781–2785, Dec. 2021.
- [7] A. Diewald et al., “Radar target simulation for vehicle-in-the-loop testing,” *Vehicles*, vol. 3, no. 2, pp. 257–271, May 2021.